

Geostatistical inversion of reflection data from thin bed coals

Jason M. McCrank, Don C. Lawton, and Cheran Mangat*

ABSTRACT

Deterministic inversion of the Alder Flats seismic data to estimate acoustic impedance has previously been completed but the band-limited results show an overestimation of the very low acoustic impedance associated with the Ardley Coals as well as an overestimation of the thickness of the coal zones. Additionally, the thin sub-zones of the Ardley Coals are not differentiated in the inversion. A geostatistical inversion was conducted in an attempt to improve the inversion resolution and assess model uncertainty. The inversion provides multiple model realizations each of which honors the seismic data, the well data and the geostatistics, and the mean of the realizations gives a highly resolved estimate of the acoustic impedance. As well, the multiple model realizations provide a range of acoustic impedance and net coal-thickness estimates that can be used to quantify uncertainty in the results. However, while the inversion appears to be accurate at the level of the shallow-most coals, at the deeper coal sub-zones a thin but significant sub-zone is not detected in the inversion, even when the inversion is constrained by the well data. This phenomenon is possibly explained by the results of synthetic modelling that investigates the effects of short-path multiple reflections. The modelling shows that the effect of short-path multiple reflections, built up in the seismic pulse from the stacked coal sub-zones, could cause a phase delay in the reflected energy of the deepest coals and could explain the results of the inversion.

INTRODUCTION

A 3D vertical component seismic survey was conducted at the Alder Flats location in June 2007. Details of the acquisition design, processing, and interpretation are discussed in McCrank and Lawton (2007a) and McCrank (2008). The data were inverted for acoustic impedance (Z_p) using several methods that are discussed in a compendium paper (McCrank and Lawton, 2008). This paper investigates a geostatistical inversion of the data using the Fugro Jason - Jason Geoscience Workbench (JGW) StatMod algorithm. Discussion of the method can be found in Torres-Verdin et al. (1999) and van der Laan and Pendrel (2001).

The 3D field layout (FIG. 1) was a square of approximately 560 x 560 m. The survey was intended to image the stratigraphy of the Ardley Coal Zone which is illustrated in the well correlation cross-section shown in FIG. 2. The Ardley Coal Zone is informally broken into the Upper and Lower Ardley coal zones (FIG. 2). The Upper Ardley is an approximately 10 m gross thickness coal zone and the Lower Ardley coal zone is represented by two thinner zones, the Silkstone coals and the deeper Mynheer coals that have gross coal thicknesses of approximately 4 m and 8 m, respectively.

* Fugro-Jason Calgary



FIG. 1. The field layout of the 3D survey.

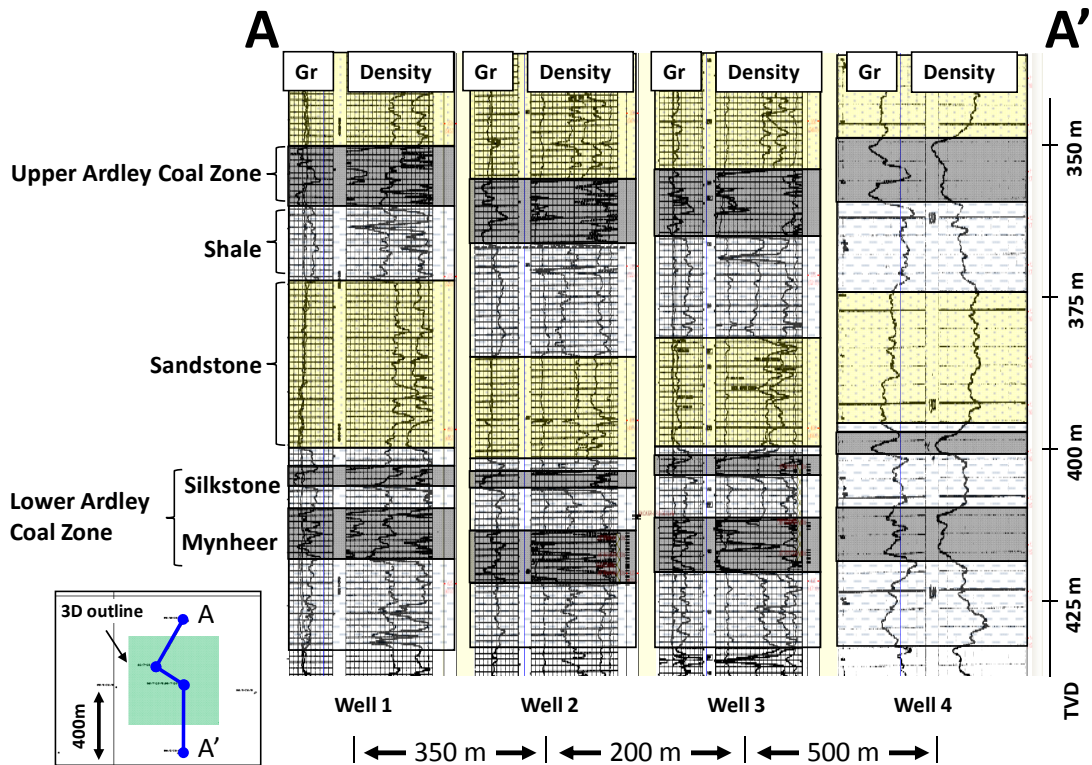


FIG. 2. An approximately 1 km long north-south geological cross-section of the Ardley Coal Zone traversing the 3D seismic volume.

Well #2 (FIG. 1 and FIG. 2) is inside the survey bounds and has high quality sonic and density logs that were used for wavelet extraction and petrophysical analysis (discussed

below). Well #3, although within the survey bounds, had a poor quality density log and no sonic log that was not used in the analysis.

The 3D volume of seismic data (FIG. 3a) contained a wavelet (FIG. 3b) that was significantly tuned in the thin but highly reflective beds of the various coal zones.

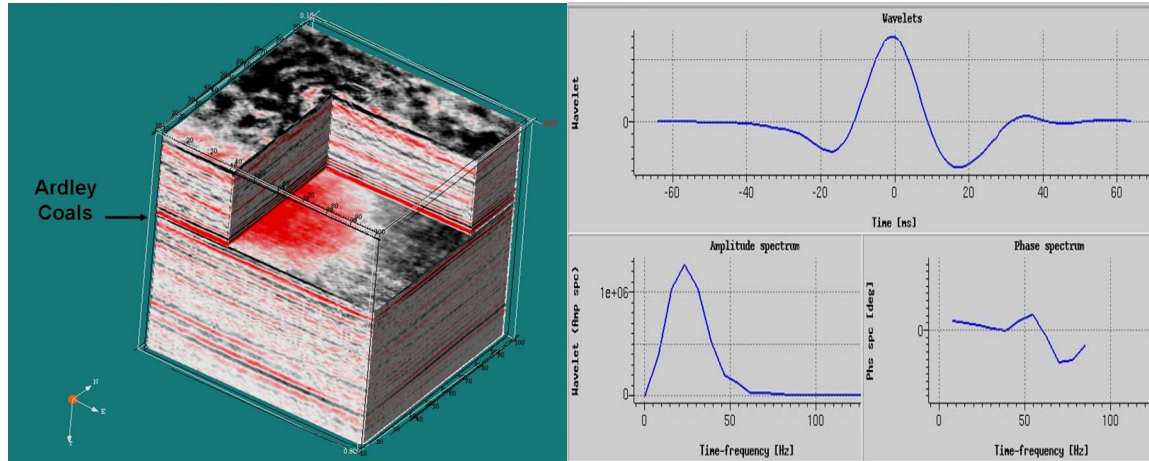


FIG. 3. (left) the 3D seismic volume and (right) the seismic wavelet.

The results from deterministic Z_p inversion

After carefully extracting a wavelet, the post-stack seismic data were deterministically inverted to estimate acoustic impedance (discussed in detail in the compendium paper, McCrank and Lawton, 2008). FIG. 4 shows a cross-section of the inverted Z_p volume. This west-east section that intersects the Well #2 shown in FIG. 4 will be the section shown in all subsequent cross-section figures in this paper.

FIG. 5 shows a cross-plot of Z_p versus gamma ray response in the well logs from Well #2. Coals can be identified with an upper limit Z_p of $6 \times 10^6 \text{ kg/m}^3 \cdot \text{m/s}$ and the lithologies with higher Z_p are defined as “clastics” (representing shales, siltstones and sandstones). The data for the cross-plot are generated at “logging” resolution as recorded in the field (resolution of approximately 15 cm to 1 m).

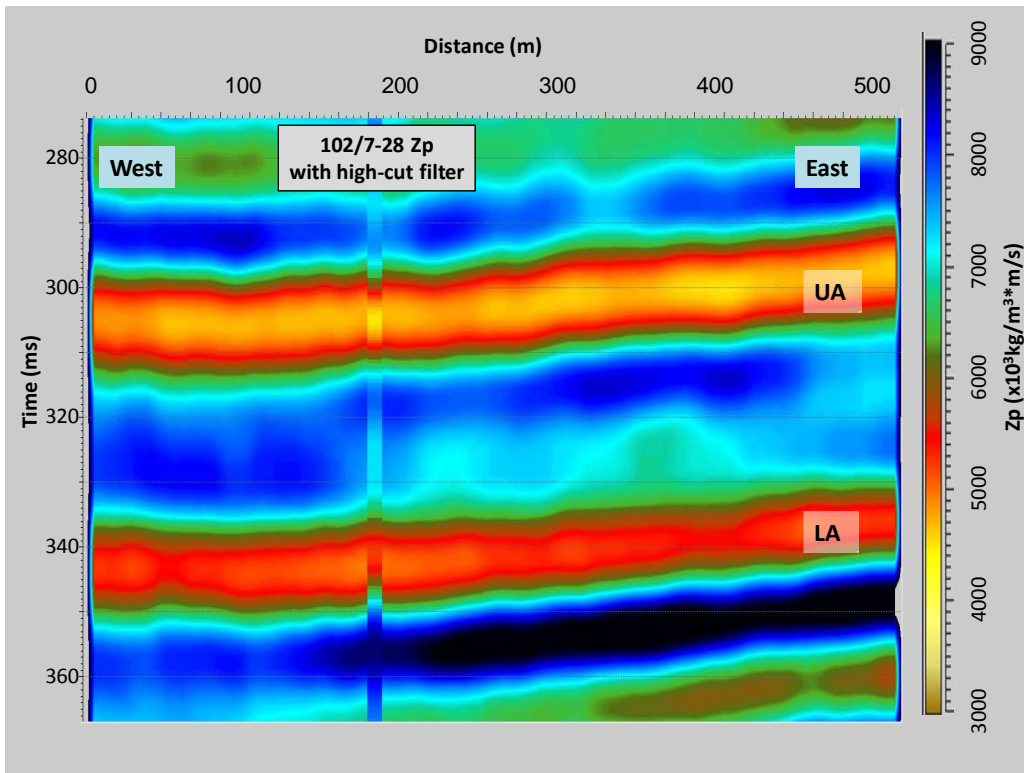


FIG. 4. A cross-section (EW) through the acoustic impedance volume that intersects Well #2. The acoustic impedance well log is superimposed on the section where the well log data have been high cut filtered at 60-70 Hz in order to match the resolution of the band-limited inverted data.

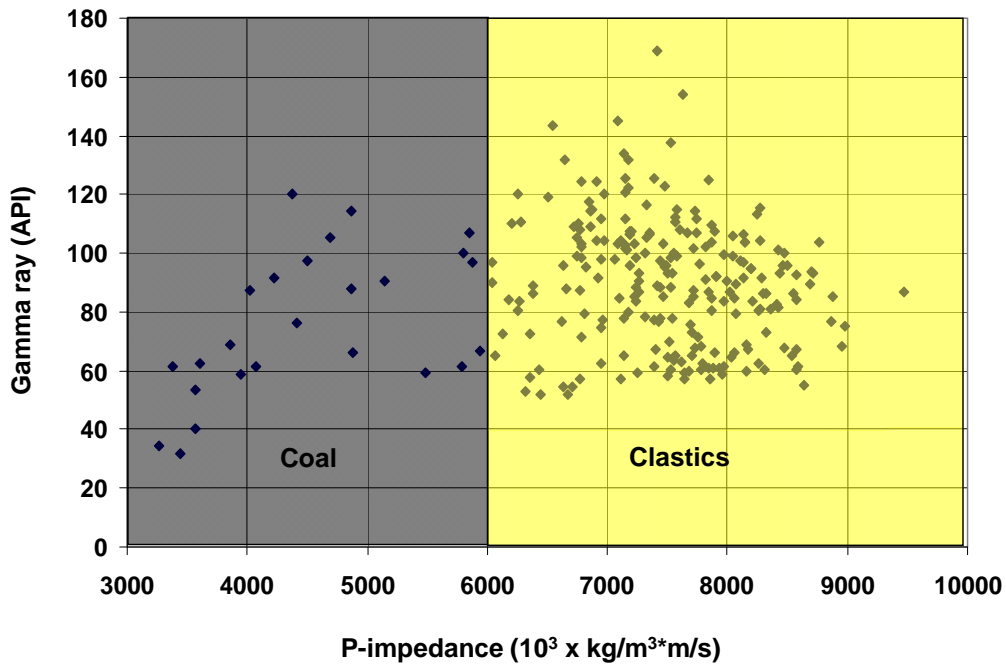


FIG. 5. Cross-plot of the acoustic impedance versus gamma ray. The coal facies is defined with acoustic impedance less than $6 \times 10^6 \text{ kg/m}^3 \cdot \text{m/s}$.

It is known that the Z_p estimate from seismic inversion will have lower band-width and less resolution than the well logs, so the cross-plot is revisited in FIG. 6 where the well log data have been logged in time (1 ms sampling) and high-cut filtered at 60-70 Hz. The lithology cut-offs are unchanged, but the resolution is diminished. The net effect can be seen in the Z_p logs and the lithology logs of FIG. 7. The Z_p log shows that the vertical detail is reduced after high-cut filtering and that the extreme amplitudes of the low Z_p coals are smoothed and increased when high cut filtered. The lithology logs resulting from these two Z_p curves are also shown in FIG. 7. It can be seen that the thin coal sub-zones in each of the Lower Ardley coal zones are “smeared” into one coal zone when the lithology is established based on the high-cut filtered Z_p log. Also, the net thicknesses of the zones in the high-cut filtered lithology log are incorrect.

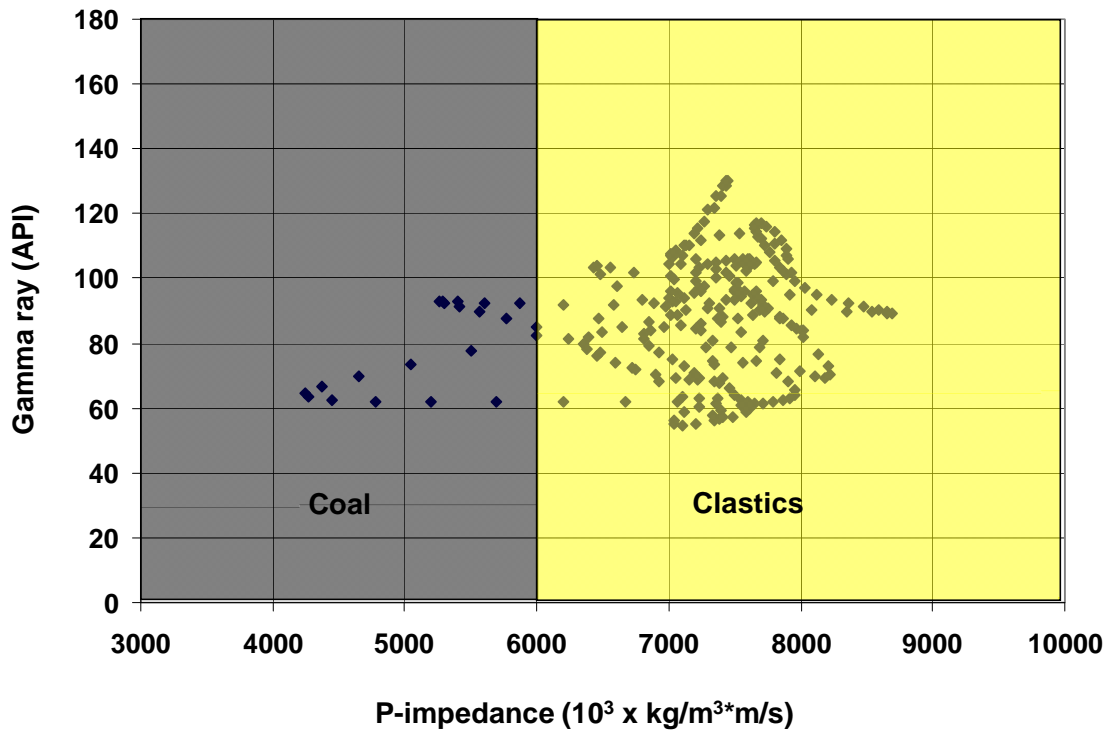


FIG. 6. Cross-plot of the acoustic impedance versus gamma ray after the well logs have been high-cut filtered at 60 Hz.

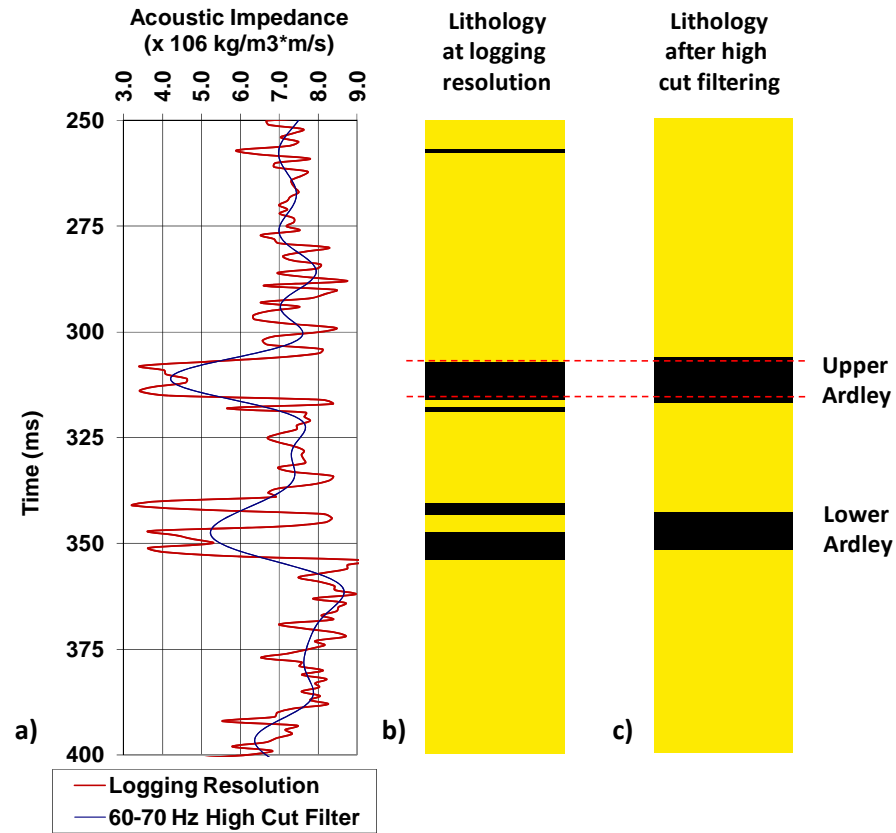


FIG. 7. (a) The Z_p log at logging resolution and after 60 Hz high-cut filtering, (b) the lithology log generated from the Z_p log at logging resolution and (c) the lithology log based on the high-cut filtered Z_p logs.

THE NEED FOR GEOSTATISTICAL INVERSION

Deterministic seismic inversions yield a result that has the maximum likelihood of being correct given the seismic data alone. However, because the Z_p estimate inverted from the seismic data is band-limited in approximately the same way that the well log data just discussed, the results will suffer from the same shortcomings. Specifically:

1. The absolute values of the Z_p estimate will be higher than the actual very low Z_p values of coal facies.
2. The thickness of the coal zones will not be accurate because at the frequency resolution of the seismic data, the low impedance of several coal zones will be smeared together and result in an “average” low Z_p inversion zone with an overestimated thickness.

These limitations are illustrated in FIG. 8 that shows the Z_p log of Well #2 at “logging” resolution superimposed on the deterministic Z_p inversion result. It is obvious that the inversion result is not capturing the detail available in the well log.

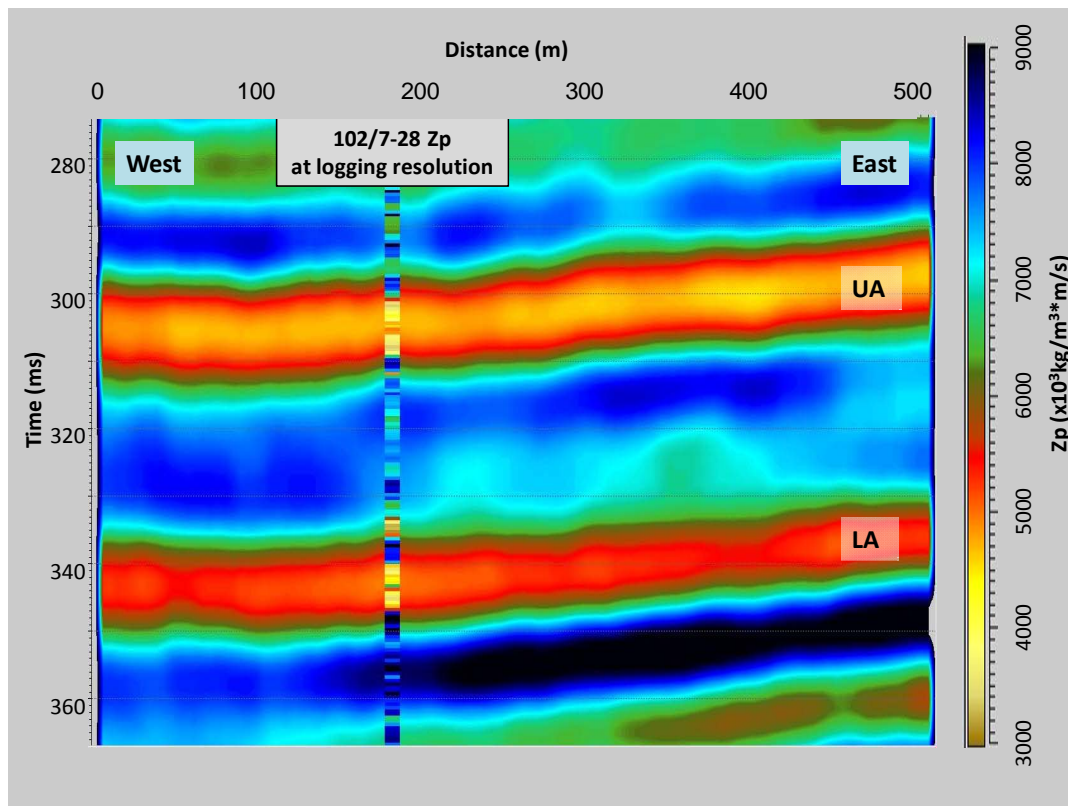


FIG. 8. The deterministic Z_p inversion results with the Z_p well log superimposed at “logging” resolution.

An additional issue that results from the band-limited Z_p inversion is that:

3. Interpretation becomes difficult because there are multiple models that could result in the same seismic response. Therefore, interpretations are not unique and the uncertainty of any interpretation can not be gauged.

In other words, due to the non-uniqueness that is endemic in inversion results, interpretations of the coal zones at resolutions higher than the Z_p estimate illustrated in FIG. 4 are difficult to defend. While none of these issues can be solved using deterministic means as there are an infinite number of models that could produce the measured data, it can not be said that each of the infinite possibilities is equally probable. The well data at high resolution can also constrain the inversion.

While the log data is known to be accurate at the well location, it provides no accuracy away from the well. However, geostatistics can provide probabilistic constraints away from the well. Geostatistical methods can not provide a unique model of the subsurface away from hard data points, but can provide probabilistic models or multiple possible realizations (i.e. from methods such as sequential Gaussian simulation). Thus geostatistical inversion proposes to solve for a set of models each of which are constrained by the available seismic data, the well data and the known geostatistics of the study area. Non-uniqueness is not eliminated but the range of possibilities and their probabilities can be estimated.

GEOSTATISTICAL INVERSION

The JGW StatMod MCTM algorithm uses the wavelet that was used in the deterministic inversion. The algorithm uses a Markov Chain Monte Carlo method to sample from the complex probabilistic density function that results from the product of the probabilities generated from the given seismic data, the well data and the geostatistical probabilities. The result of the inversion is a set of high resolution model realizations each of which match the seismic and the geostatistical constraints that are input to the inversion. The results are a representative sampling of the Bayesian posteriori probabilistic density function.

Histograms of the Z_p values for each of the two facies (coal and clastics) were generated from the well logs (FIG. 9). Also, the vertical variograms for the facies and Z_p values were modeled using the well data (FIG. 10). The Z_p variance was modelled by an exponential variogram and the facies variance was modelled as a Gaussian variogram. The range of all vertical variograms was approximately 2 ms.

A lack of lateral data made it impossible to empirically model the lateral variograms, so the range and model were estimated by running the inversion repeatedly until the results matched an intuitive belief about the variation of the facies and the Z_p values given the regional geology and demonstration cross-sections such as that shown in FIG. 2. It was found that when the lateral facies variance was again modelled with a Gaussian variogram and the Z_p variance modelled with an exponential variogram, the results were robust as long as the range was set between 200 – 800 m. For the final inversion the range was set to 400 m.

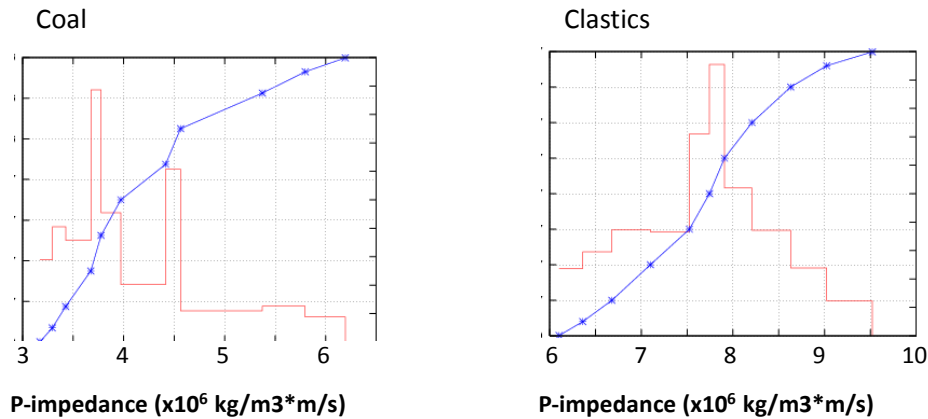


FIG. 9. Z_p histograms for each facies.

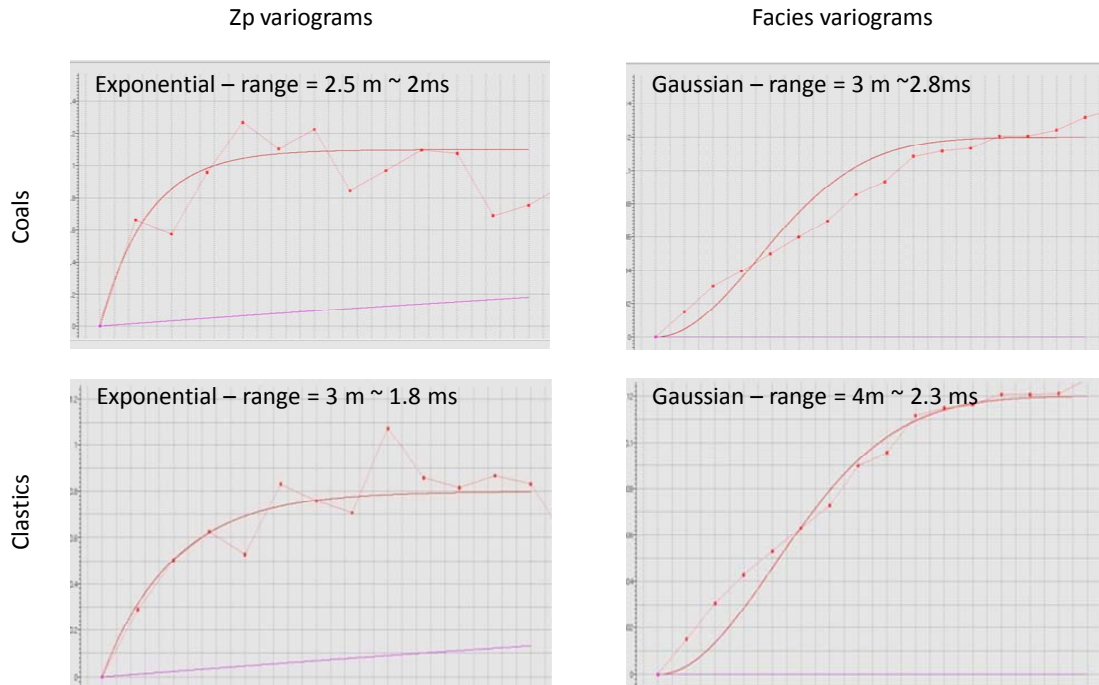


FIG. 10: The vertical variograms for Zp and facies for each of the two facies.

INVERSION UNCONSTRAINED BY THE WELL

The inversion can be run with or without the Zp well log used as a constraint. Initially, the inversion was conducted without well constraint in order to understand how much detail was being provided by the seismic data and the geostatistics alone. The inversion was run to find 10 model realizations. FIG. 11 shows cross-sections of the resulting Zp estimates. The panel on the upper left is the average Zp estimate after generating 10 model realizations from the Markov Chain Monte Carlo algorithm. Five of these ten realizations (selected arbitrarily) are illustrated in the other five panels of FIG. 11. Superimposed on each of the panels is the Zp well log from Well #2 that has not been filtered and is displayed at “logging” resolution. The inversion results show that the level of detail in the Zp estimates is comparable to the well log resolutions. Also, the absolute Zp values of the inversion are comparable to the absolute Zp values of the unfiltered well log.

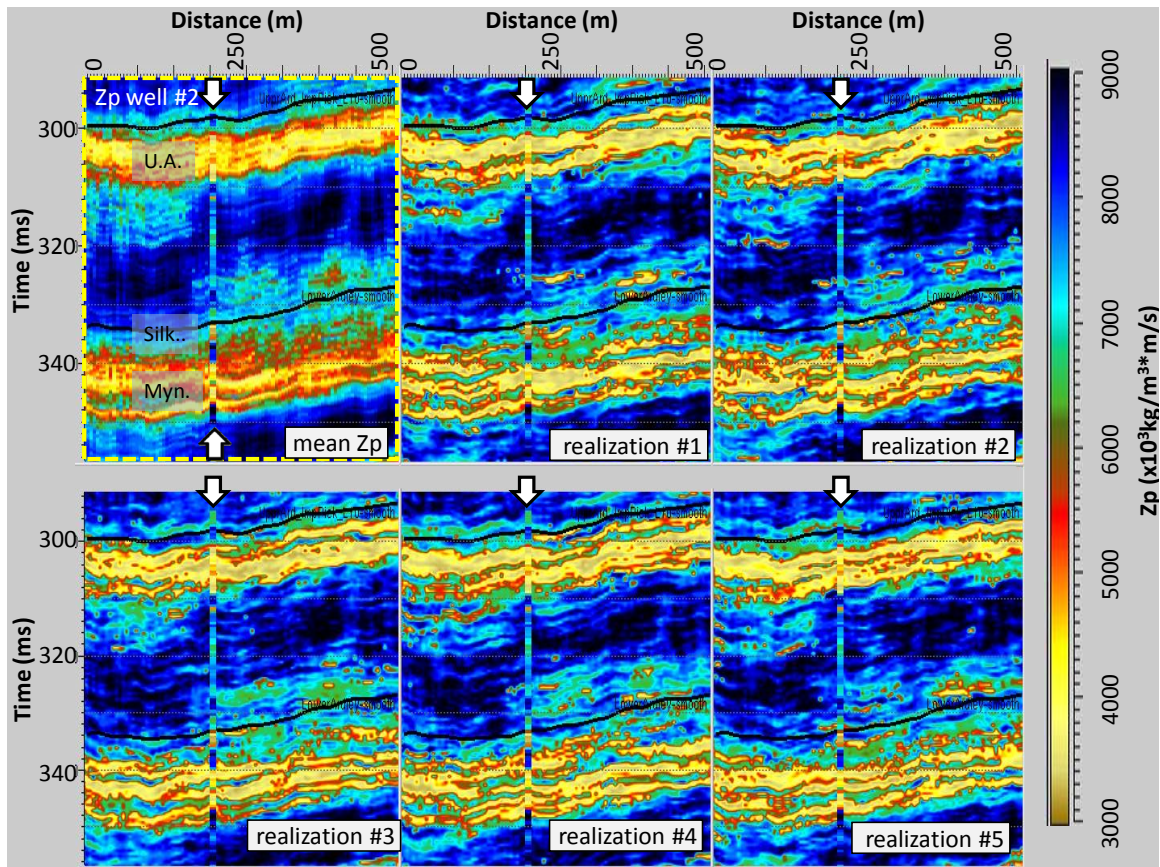


FIG. 11. The unconstrained Z_p inversion results. The cross-section in the upper left is the mean Z_p of 10 inversion realizations. The other 5 cross-sections are an arbitrary sampling of 5 of the 10 realizations.

Each of the 10 realizations should be viewed as possible model solution to the inversion. FIG. 12 illustrates the residual difference between the seismic data and the synthetic seismogram generated from one of the 10 model realizations. The figure shows that the residual difference is very small. Each of the 10 realizations shows an equally minimal residual meaning that each is an inversion that is compatible with the seismic data.

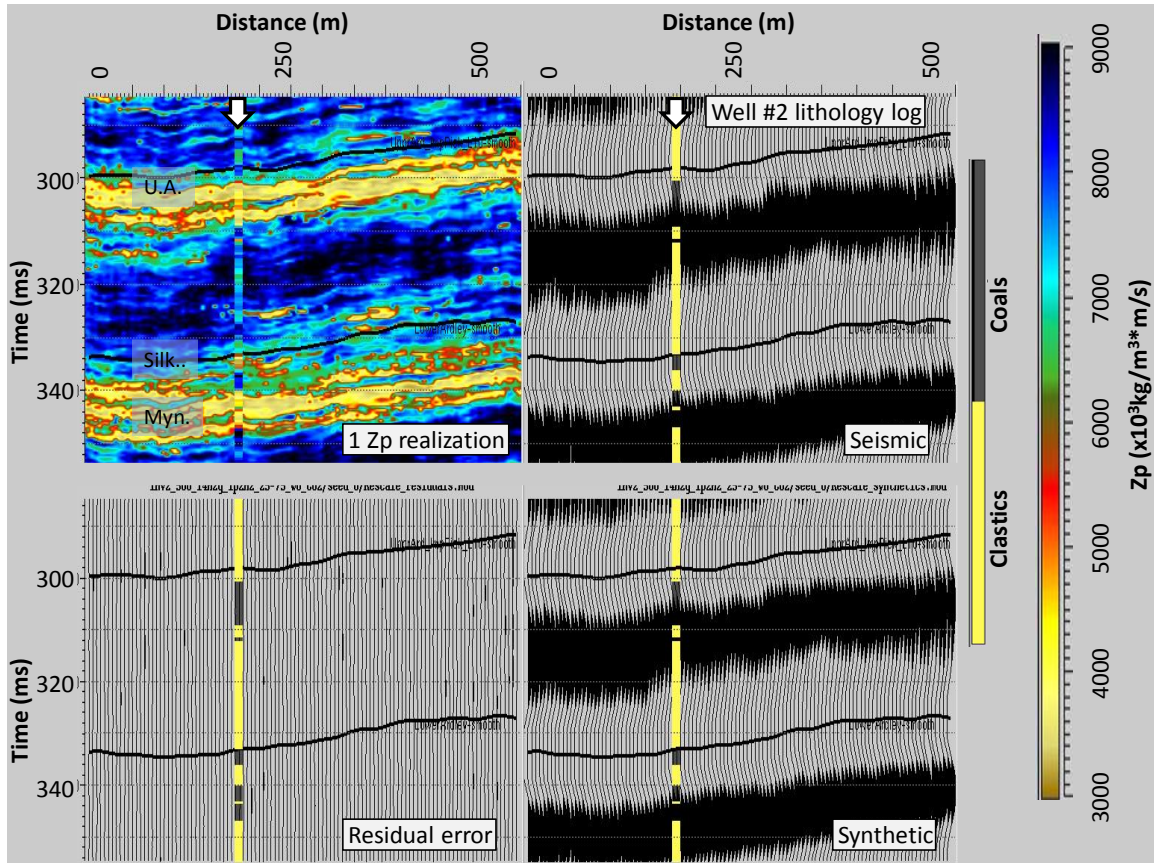


FIG. 12. Analysis of one arbitrary realization. (a) The Z_p realization, (b) the original seismic data, (c) the residual difference between the seismic data and the synthetic seismogram generated from the Z_p model realization and (d) the synthetic seismogram generated from the Z_p model realization.

The most likely facies estimate is shown in the panel on the upper left of FIG. 13, and the other five panels show the facies associated with the five realizations from FIG. 11. The figure shows that the statistical form of the coal zones appears to be modelled in each realization. Each of the individual realizations shows very small coal occurrences in locations that are outside of the expected coal zones, however, when these realizations are averaged to produce the most probable facies, coals are predicted in the known zones only. In the most probable facies panel, continuous but distinct thin coal zones are resolved. However, while the Upper Ardley coal zone appears to be accurately resolved, the Lower Ardley coal zone is not. In the Lower Ardley coal zone, the most probable facies results appear to show two sub-zones but these are together delayed in time and the Silkstone coal zone is not resolved at all.

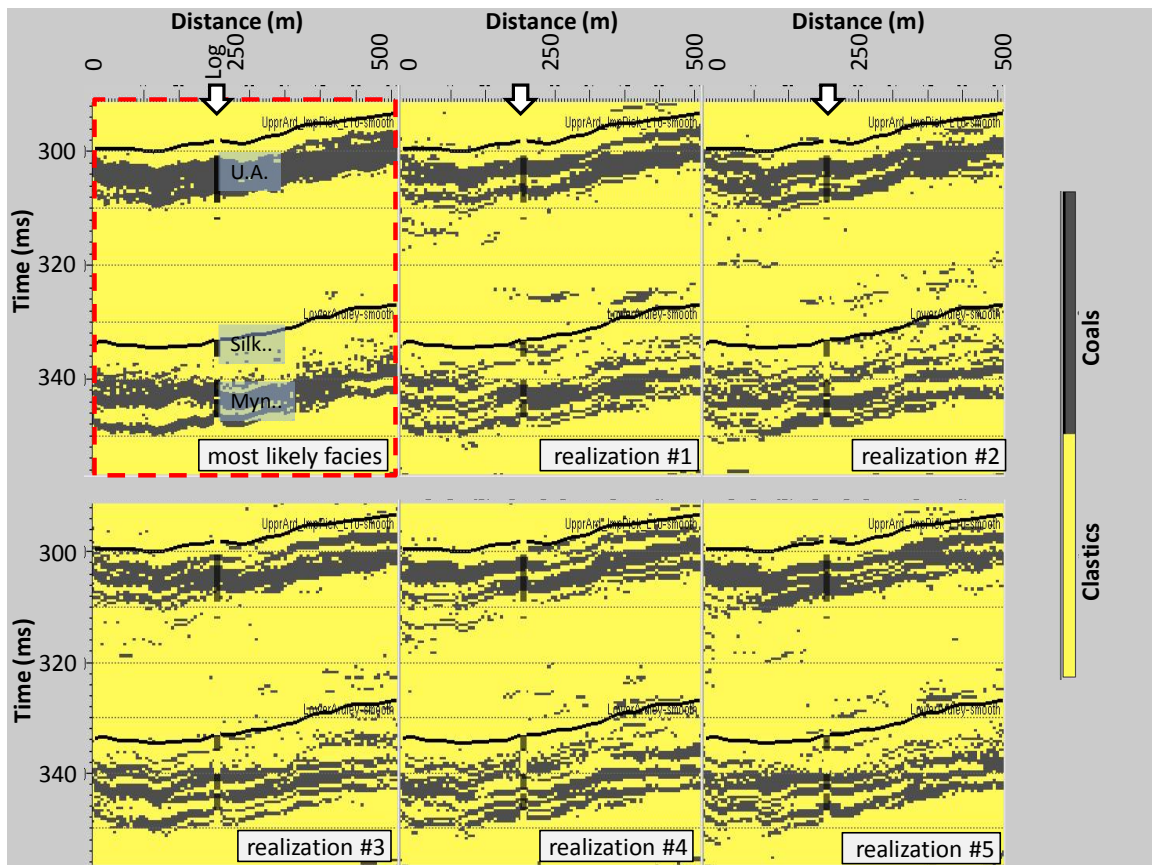


FIG. 13. The unconstrained inversion facies results. The cross-section in the upper left is the most likely facies of 10 inversion realizations. The other 5 cross-sections are an arbitrary sampling of 5 of the 10 realizations.

FIG. 14 summarizes the results of the unconstrained inversion. It shows the deterministic inversion results (for comparison) as well as the most probable facies, the likelihood of coal facies, and the minimum, mean and maximum Z_p from the set of model realizations. The probability of coal is high in each of the coal zones and this data can be used to give a quantitative understanding of the likelihood of encountering different gross thicknesses of coal. Again the results are robust for the Upper Ardley coal zone but indicate greater uncertainty in the Lower Ardley coal zone. The data seems to suggest that the existence of the Silkstone coal zone is improbable, since there is a very low probability of coal facies at that level.

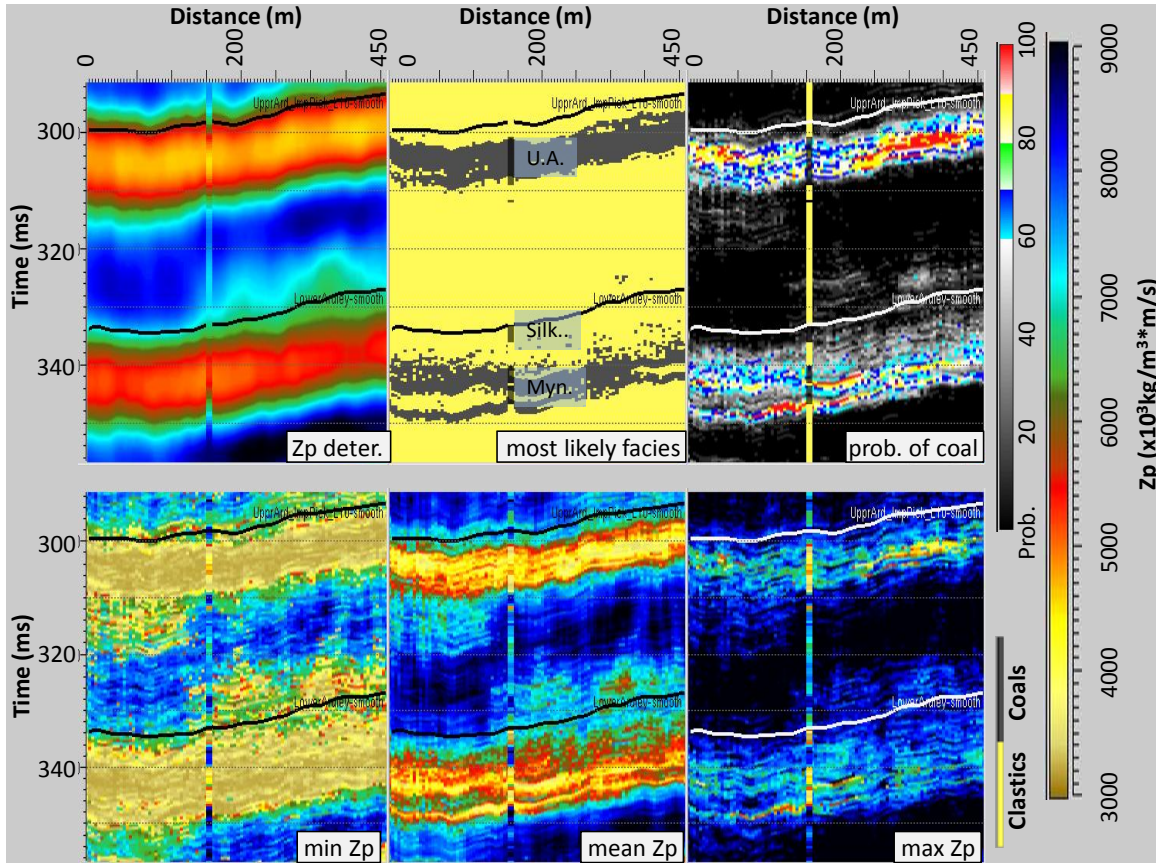


FIG. 14. A summary of the unconstrained inversion results. (a) The results of the deterministic inversion (for comparison), (b) the most likely facies, (c) the probability of coal facies, (d) the minimum Z_p estimate of the 10 realizations, (e) the mean Z_p of the 10 realizations and (f) the maximum Z_p estimate of the 10 realizations.

THE INVERSION CONSTRAINED BY THE WELL

The inversion was then run with the Z_p values and the facies log of Well #2 included as a constraint on the geostatistical realizations. Again, the inversion found 10 possible model realizations that are each constrained by the well data, the geostatistics and the seismic data. FIG. 15 shows the residual difference between the seismic data and the synthetic seismogram created from one of the realizations. It shows that the residual is again very small. It is noteworthy that the Silkstone coal zone is a part of the model solution at least at and near the Well #2 location.

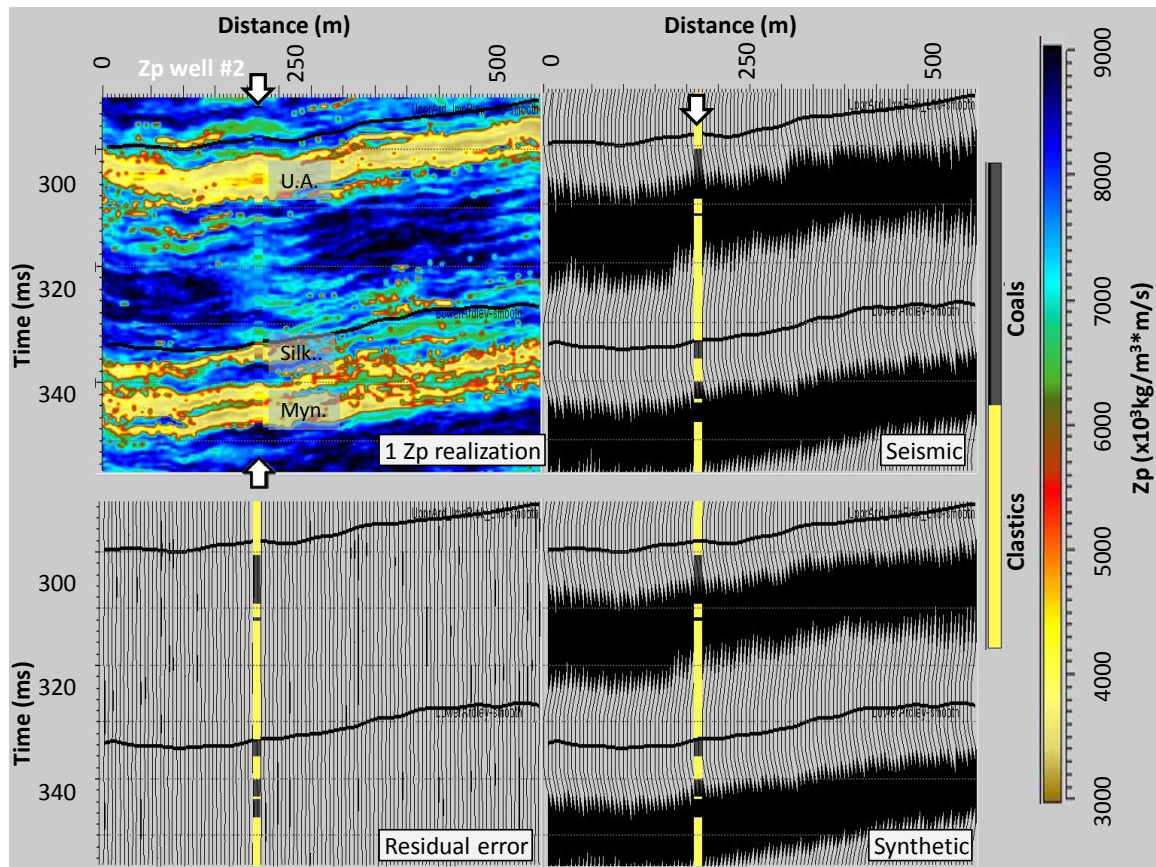


FIG. 15. Analysis of one arbitrary realization with the Z_p of Well #2 (shown) as a constraint. (a) The Z_p realization, (b) the original seismic data, (c) the residual difference between the seismic data and the synthetic seismogram generated from the Z_p model realization and (d) the synthetic seismogram generated from the Z_p model realization.

FIG. 16 shows nine of the ten realizations along with the facies log from Well #2. As in the unconstrained results, the absolute Z_p values of the inversion match those of the well log with coal zones showing Z_p values as low as $3.0 \times 10^6 \text{ kg/m}^3 \cdot \text{m/s}$. Each of the realizations shows evidence of the Silkstone coal zone at or near the Well #2 location, but in each realization the low Z_p zone of these coals disappears away from the well.

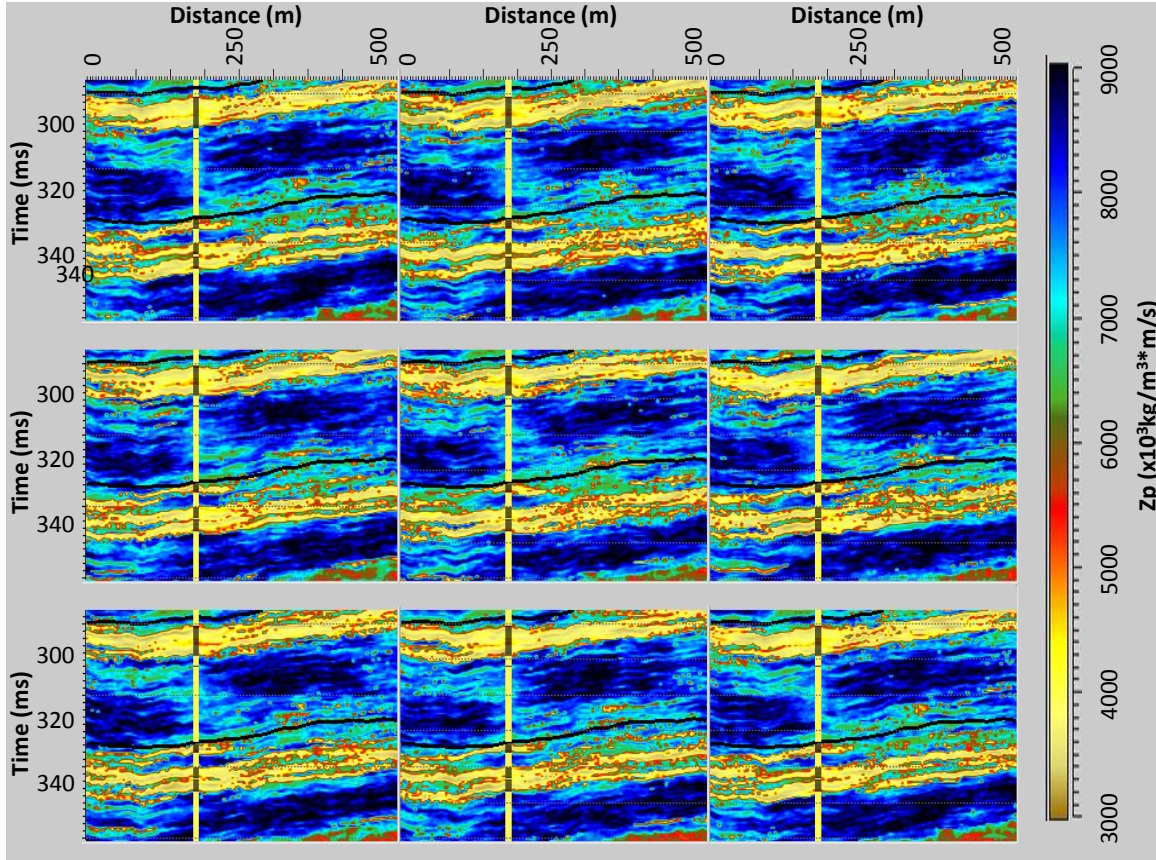


FIG. 16. Nine of the ten Z_p model realizations constrained by the Well #2 Z_p well log (shown as a facies log for visualization purposes).

FIG. 17 shows the mean Z_p estimate of the 10 realizations and FIG. 18 shows the associated most probable facies generated from the inversion with well constraint. Again, the expected continuity and thickness of the coal zones is produced.

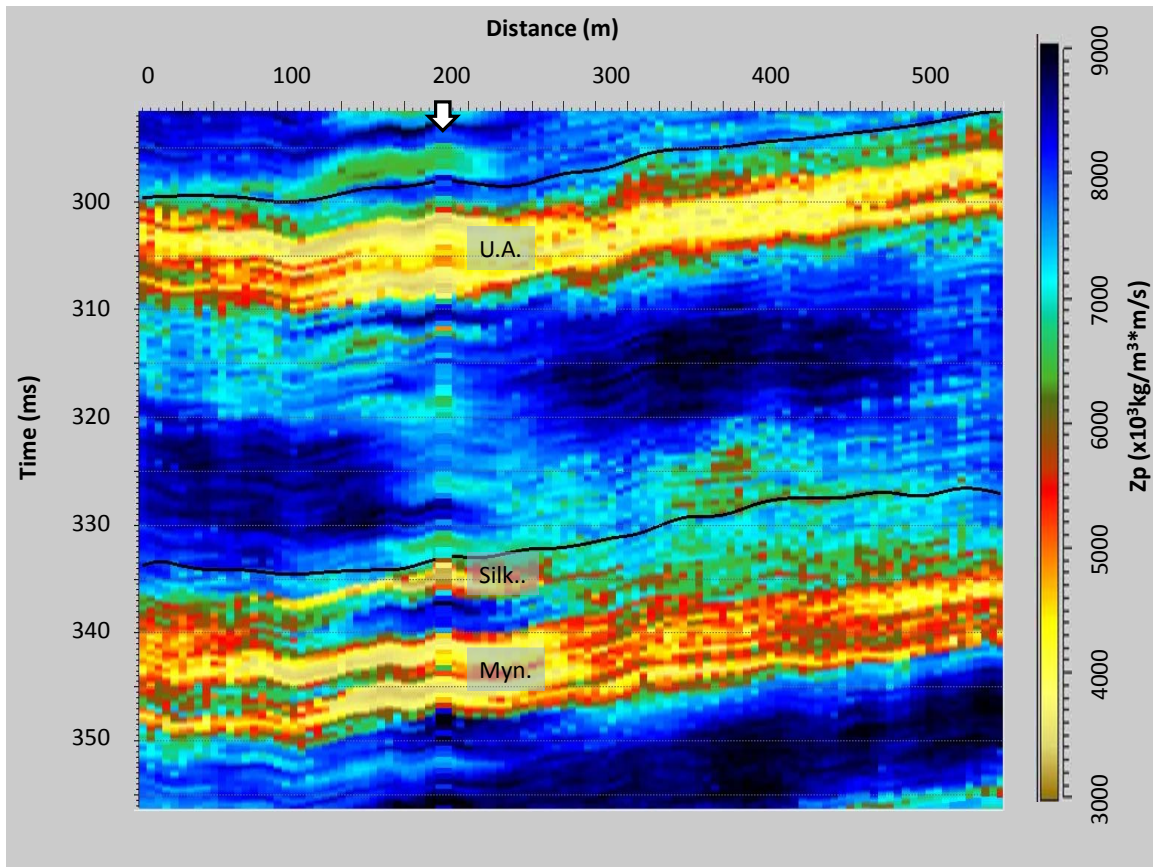


FIG. 17. The mean Z_p estimate of the 10 constrained realizations with the Z_p well log from Well #2 superimposed.

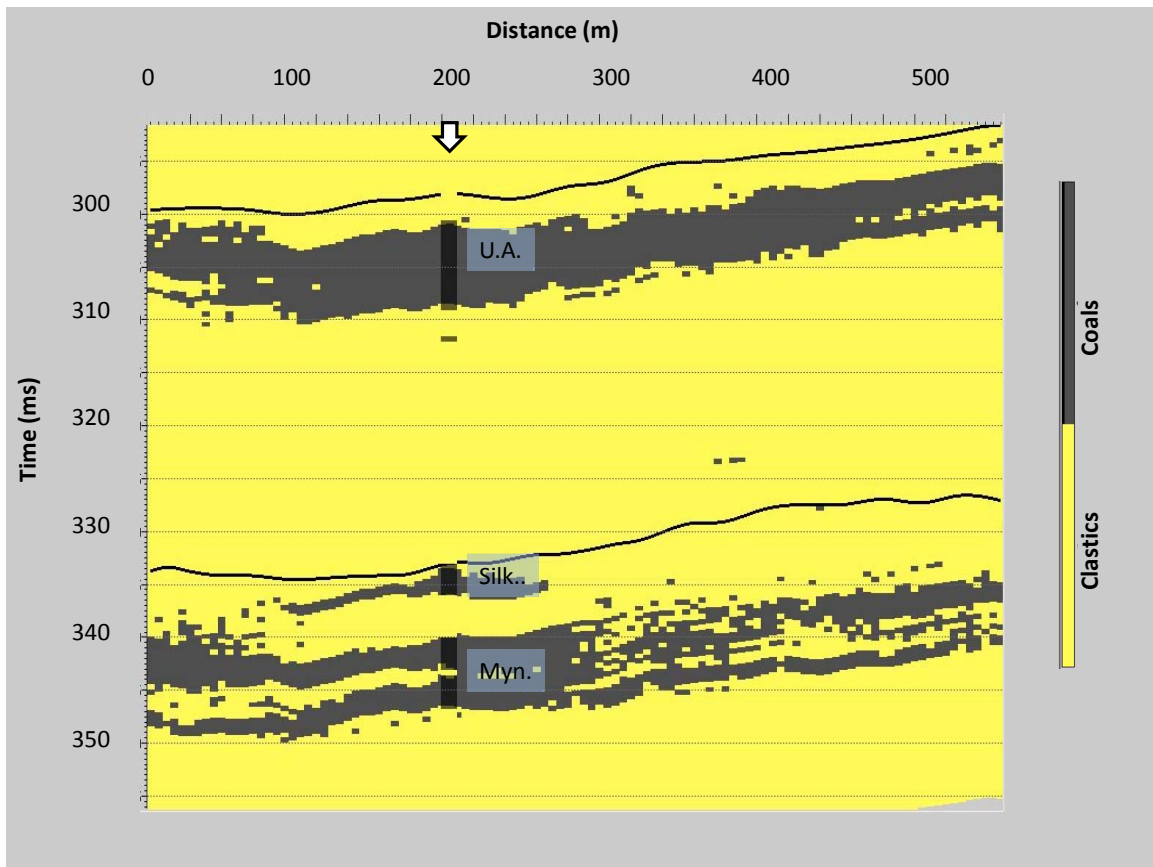


FIG. 18. The most probably facies realization from the 10 realizations constrained by the Well #2 facies (shown).

FIG. 19 shows a summary of the constrained inversion results. The panel in the upper right illustrates the probability of coal facies existence and shows that the probability of coal is highest closest to the well location and decreases at distance from the well. Such information can be used to add the dimension of quantified uncertainty in the inversion result.

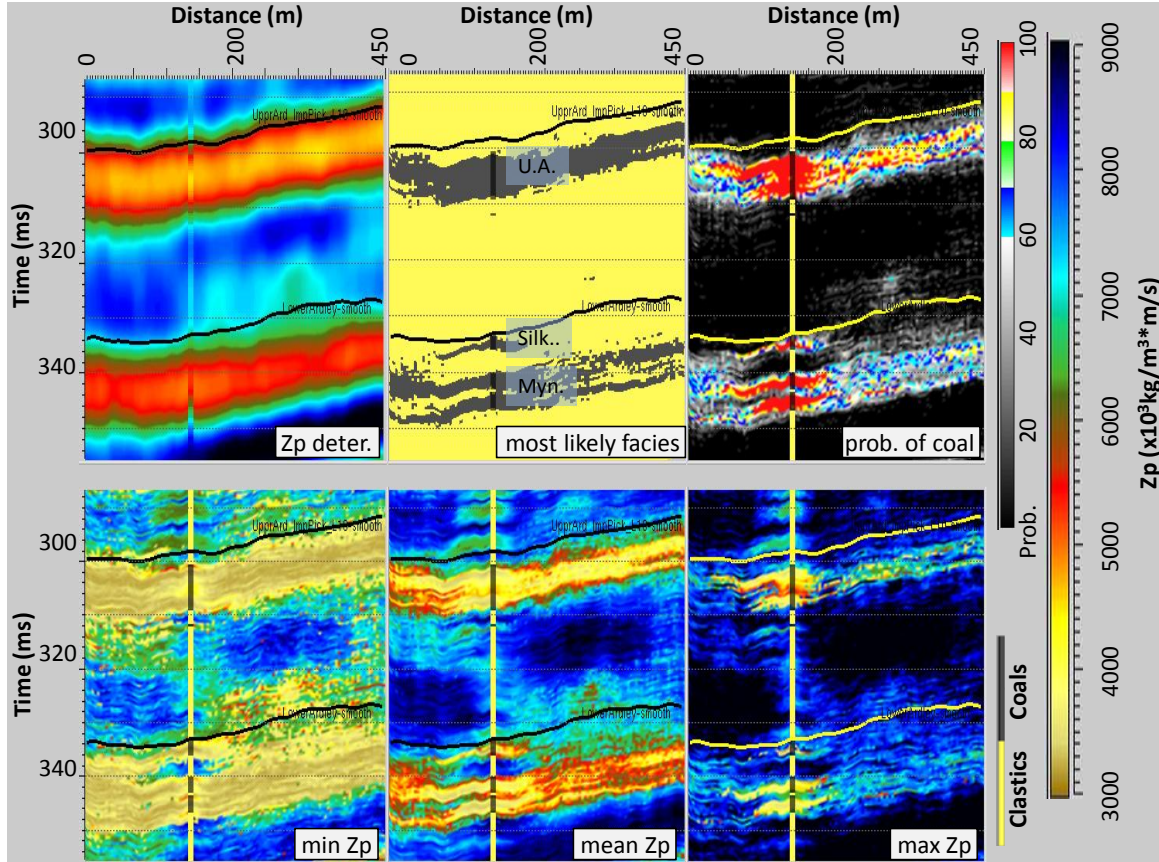


FIG. 19. A summary of the constrained inversion results. (a) The results of the deterministic inversion (for comparison), (b) the most likely facies, (c) the probability of coal facies, (d) the minimum Z_p estimate of the 10 realizations, (e) the mean Z_p of the 10 realizations and (f) the maximum Z_p estimate of the 10 realizations.

FIG. 20 illustrates the comparison of the mean Z_p and most probable facies results for the constrained and unconstrained inversions. The figure shows that the constrained inversion clearly honors the well data where the unconstrained results do not. However, both are comparable in terms of the coal zone thicknesses and lateral continuity.

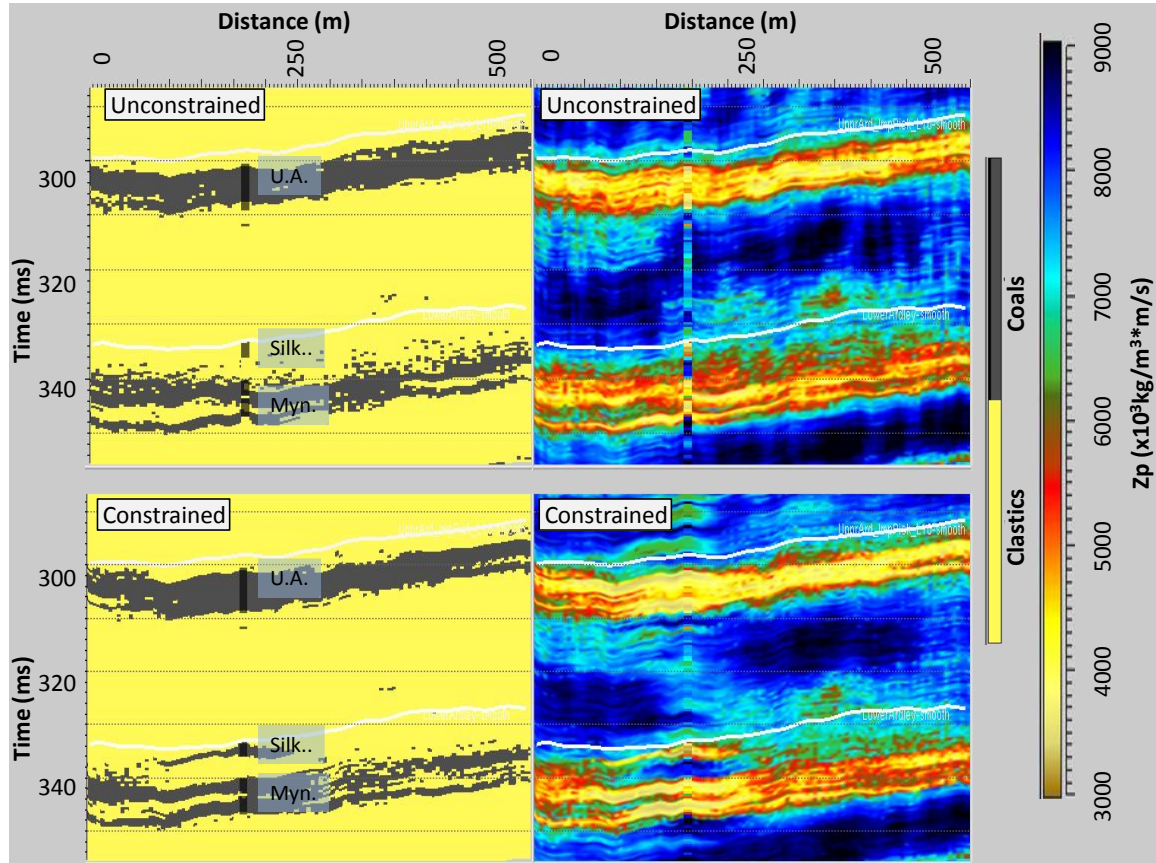


FIG. 20. A comparison of the constrained and the unconstrained inversion results showing the most probable facies (left) and mean Z_p (right).

The Upper Ardley coal zone is well characterized in the constrained inversion; however, the Lower Ardley coal zone character is more problematic. While the Silkstone coal zone is predicted at and near the Well #2, it disappears within 50 – 100 m away from the well. Thus it appears that the seismic data is overriding the likely geostatistical prediction at a distance of less than a quarter of the lateral variogram range (400 m). In other words, the seismic data does not predict the existence of the Silkstone coals. The likely explanations for this are there is a fundamental flaw with the seismic trace waveform, the wavelet may not be accurate or the time-to-depth table for the well log may be incorrect. However, given that the inversion works very well for the Upper Ardley coal zone, it may be that the problem is localized to the seismic event of the Lower Ardley coals.

A possible explanation comes from Schoenberger and Levin (1974 and 1978) who investigated the effect of short-path multiples on the seismic response of cyclically bedded coal seams. They showed an example (replicated in FIG. 21) where the energy of the primary reflection from coals deep in a cyclic series of coal cyclothem was

overpowered by the energy from inter- and intra-bed short-path multiples. The net effect is a delay in the arrival time of the peak energy of the reflections.

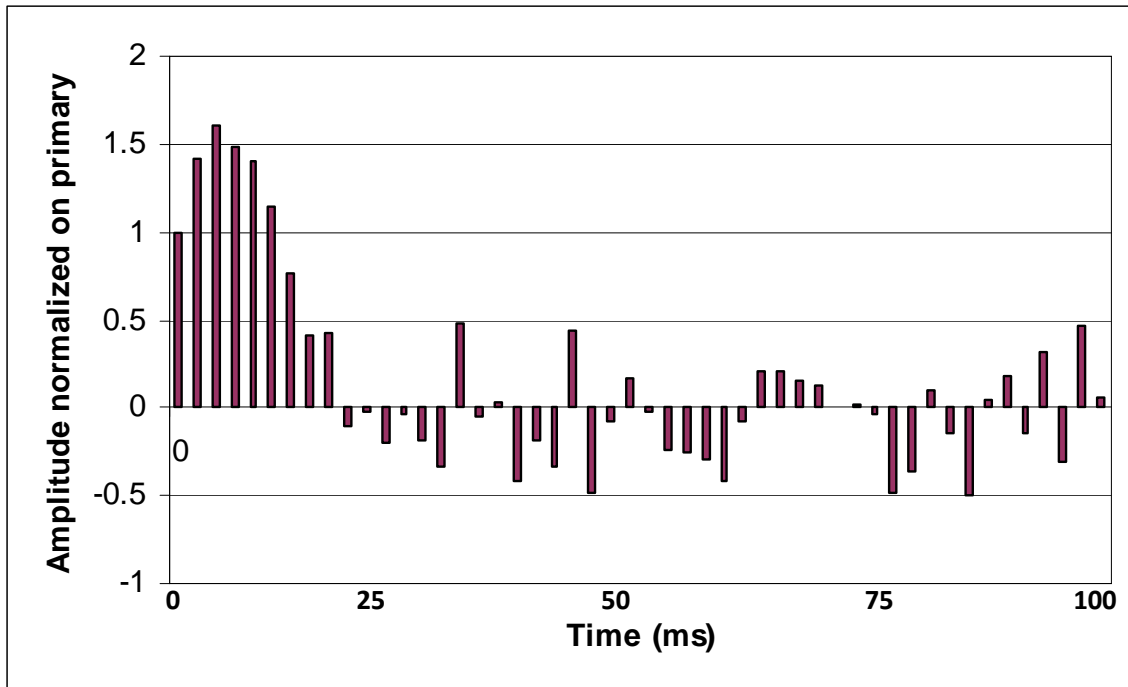


FIG. 21. An example illustrating the energy of a primary pulse at time zero and the energy of short-path multiple reflections for a signal that has passed through a series of coal beds. The examples shows how the initial pulse is dominated by the delayed arrivals of pulses from the short-path multiples (after Schoenberger and Levin, 1974).

To investigate whether short-path multiples play a role in the trace wave form of the Alder Flats data, offset gathers were synthesized with the reflectivity method. The method models the full waveform response of the earth and can be calculated with or without including multiples and mode conversions. The results are illustrated in FIG. 22 which shows the offset gathers with NMO removed and the stacks of the modelled gathers. In the stack that includes all multiple and mode conversion reflections, there is a slight phase delay (3-5 ms) in the onset of the reflection event that ties to the base of the Lower Ardley coals. This delay corresponds to the scale of delay that would be required to explain why the inversion result is unable to predict the location of the Silkstone coals.

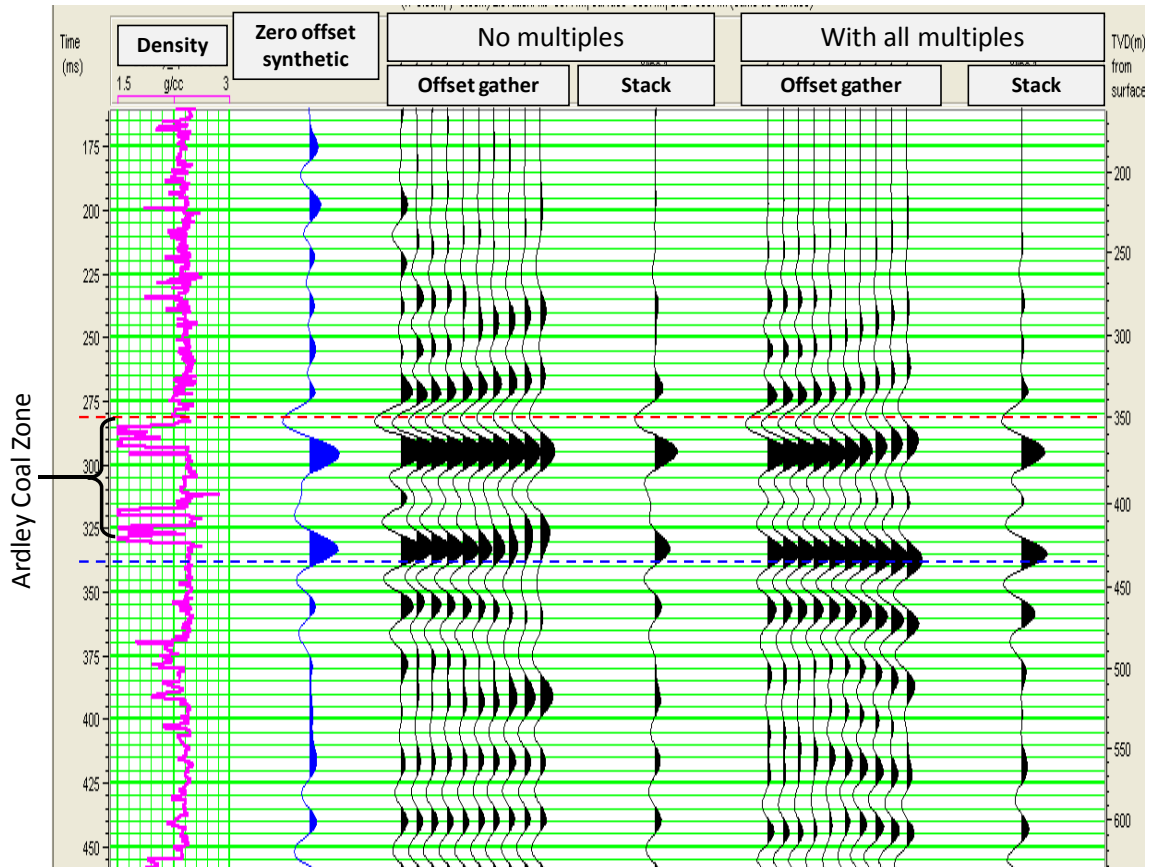


FIG. 22. Synthetic seismograms showing the effect of short-path multiples and mode conversions by comparing gathers and stacks with and without including multiples in the model. All models were created with a zero-phase 5-10-50-60 Hz Ormsby wavelet. The dotted lines are constant time lines for comparing the phase of the different models.

CONCLUSIONS

The geostatistical inversion successfully improved the Z_p inversion result in the Upper Ardley coals. The absolute estimated Z_p values were equivalent to the values from the well logs at logging resolution and bed thicknesses were accurately predicted. In addition, since each of realizations is consistent with the seismic data and is a possible representation of the earth model, the range of Z_p values and coal zone net-thicknesses that are captured by the realizations allow the uncertainty of the coal characteristics to be assessed. For example, the probability of achieving a certain coal net-thickness could be calculated from the multiple realizations.

While the unconstrained inversion was unable to detect the thin Silkstone coal zone, and even the constrained inversion did not produce a convincing representation of the Silkstone coal zone, the inversion results remain interesting. That the inversion could not detect the Silkstone coal zone is indicative of a problem with the data at the localized level of the Lower Ardley coals which is itself a useful conclusion.

ACKNOWLEDGEMENTS

The author would like to thank Fugro-Jason for allowing me to use the Jason Geoscience Workbench and its many tools to conduct this work. The gracious assistance of the staff of the Fugro-Jason Calgary office, especially John Pendrel, Cheran Mangat, Jawwad Ahmad, Brian Hoffe and Olga Rehkopf is very much appreciated.

Also of critical importance is to thank the CREWES sponsors, the volunteers and workers who contributed to the field acquisition, and the dedicated faculty, staff, and students of CREWES and the University of Calgary Geoscience Department for assistance, discussion and inspiration. Finally, Hampson Russell Software was used to conduct synthetic reflectivity modelling.

REFERENCES

- McCrank, J.M., 2008, MSc Thesis, University of Calgary: yet to be published.
- McCrank, J.M. and Lawton, D.C., 2007, Alder Flats 2D and 3D Seismic Programs, CREWES Research Report, **19**.
- McCrank, J.M. and Lawton, D.C., 2008, Acoustic Impedance Inversion and CO2 Detection at Alder Flats, CREWES Research Report, **20**.
- Schoenberger, M., Levin, F.K., 1974, Apparent attenuation due to interbed multiples: Geophysics, **39**, 278-291.
- Schoenberger, M., Levin, F.K., 1978, Apparent attenuation due to interbed multiples, II: Geophysics, **43**, 730-737.
- Torres-Verdin, C., Victoria, M., Pendrel, J., 1999, Trace-based and geostatistical inversion of 3-D seismic data for thin-sand delineation: An application in San Jorge Basin, Argentina: The Leading Edge, No. 9.
- Van der Laan, J., Pendrel, J., 2001, Geostatistical simulation of porosity and risk in a Swan Hills reef, SEG International Exposition and Annual Meeting Expanded Abstracts, September 2001.